Measurements of the Branching Fraction, Polarization, and *CP* Asymmetry for the Decay $B^0 \to \omega\omega$

Y. Guan, A. J. Schwartz, K. Kinoshita, I. Adachi, H. Aihara, S. Al Said, D. M. Asner, H. Atmacan, R. Ayad, S. Bahinipati, Sw. Banerjee, K. Belous, J. Bennett, M. Bessner, V. Bhardwaj, B. Bhuyan, D. Biswas, A. Bobrov, D. Bodrov, J. Borah, A. Bozek, M. Bračko, P. Branchini, T. E. Browder, A. Budano, M. Campajola, L. Cao, D. Červenkov, M.-C. Chang, P. Chang, B. G. Cheon, K. Chilikin, H. E. Cho, K. Cho, S.-K. Choi, Y. Choi, S. Choudhury, S. Das, G. De Nardo, G. De Pietro, R. Dhamija, F. Di Capua, J. Dingfelder, Z. Doležal, T. V. Dong, S. Dubey, P. Ecker, D. Epifanov, T. Ferber, D. Ferlewicz, B. G. Fulsom, V. Gaur, A. Giri, P. Goldenzweig, E. Graziani, T. Gu, K. Gudkova, C. Hadjivasiliou, K. Hayasaka, H. Hayashii, S. Hazra, M. T. Hedges, W.-S. Hou, C.-L. Hsu, N. Ipsita, A. Ishikawa, R. Itoh, M. Iwasaki, W. W. Jacobs, S. Jia, Y. Jin, K. K. Joo, T. Kawasaki, C. H. Kim, D. Y. Kim, K.-H. Kim, Y. J. Kim, Y.-K. Kim, P. Kodyš, A. Korobov, S. Korpar, E. Kovalenko, P. Križan, P. Krokovny, T. Kuhr, R. Kumar, K. Kumara, T. Kumita, Y.-J. Kwon, Y.-T. Lai, S. C. Lee, D. Levit, L. K. Li, Y. Li, Y. B. Li, L. Li Gioi, J. Libby, D. Liventsev, T. Luo, M. Masuda, T. Matsuda, S. K. Maurya, F. Meier, M. Merola, F. Metzner, K. Miyabayashi, R. Mizuk, G. B. Mohanty, R. Mussa, I. Nakamura, M. Nakao, Z. Natkaniec, A. Natochii, L. Nayak, M. Nayak, M. Niiyama, S. Nishida, S. Ogawa, H. Ono, G. Pakhlova, S. Pardi, H. Park, J. Park, S.-H. Park, S. Paul, R. Pestotnik, L. E. Piilonen, T. Podobnik, E. Prencipe, M. T. Prim, M. Röhrken, G. Russo, S. Sandilya, L. Santelj, V. Savinov, G. Schnell, C. Schwanda, Y. Seino, K. Senyo, M. E. Sevior, W. Shan, J.-G. Shiu, E. Solovieva, M. Starič, K. Sumisawa, M. Takizawa, U. Tamponi, K. Tanida, F. Tenchini, R. Tiwary, K. Trabelsi, M. Uchida, Y. Unno, S. Uno, P. Urquijo, Y. Usov, S. E. Vahsen, K. E. Varvell, A. Vinokurova, M.-Z. Wang, S. Watanuki, E. Won, X. Xu, B. D. Yabsley, W. Yan, Y. Yook, L. Yuan, Z. P. Zhang, V. Zhilich, and V. Zhukova

(Belle Collaboration)

We present a comprehensive study of $B^0 \to \omega\omega$ decays using 772×10^6 $B\bar{B}$ pairs collected with the Belle detector at the KEKB e^+e^- collider. This process is a suppressed charmless decay into two vector mesons and can exhibit interesting polarization and *CP* violation. The decay is observed for the first time with a significance of 7.9 standard deviations. We measure a branching fraction $\mathcal{B} = (1.53 \pm 0.29 \pm 0.17) \times 10^{-6}$, a fraction of longitudinal polarization $f_L = 0.87 \pm 0.13 \pm 0.13$, and a time-integrated *CP* asymmetry $A_{CP} = -0.44 \pm 0.43 \pm 0.11$, where the first uncertainties listed are statistical and the second are systematic. This is the first observation of $B^0 \to \omega\omega$ and the first measurements of f_L and A_{CP} for this decay.

DOI: 10.1103/PhysRevLett.133.081801

In the standard model (SM), the decay $B^0 \to \omega\omega$ proceeds via a $\bar{b} \to \bar{u}$ spectator amplitude and a $\bar{b} \to \bar{d}$ loop ("penguin") amplitude [1]. Interference between these two amplitudes, which have different weak and strong phases, gives rise to direct *CP* violation. This *CP* asymmetry is sensitive to the internal angle (or phase difference) $\phi_2 \equiv \arg[-(V_{tb}^* V_{td})/(V_{ub}^* V_{ud})]$ of the Cabibbo-Kobayashi-Maskawa (CKM) unitarity triangle [2–4]. Measuring ϕ_2 tests the unitarity of the CKM matrix; if the matrix was found to be nonunitary, that would imply physics beyond the SM.

Another observable sensitive to new physics is the fraction of longitudinal polarization (f_L). The fraction f_L measured for the vector-vector (VV) decay $B \to \phi K^*$ is surprisingly small [5–9]; this triggered much interest in VV decays. Numerous explanations of this anomaly have been proposed, e.g., penguin-annihilation amplitudes [10], enhanced electroweak penguins [11,12], and also new physics scenarios [13,14]. The fraction f_L measured for

the $\bar{b} \to (\bar{u}, \bar{d})$ decay $B^0 \to \rho^0\rho^0$ [15–19], which is color suppressed, is also unexplained; measurement of f_L for $B^0 \to \omega\omega$, also color suppressed, could give insight into QCD dynamics and help solve this puzzle.

For $B \to VV$ decays, there are three possible polarization states: the longitudinal state with amplitude H_0 and two transverse states with amplitudes H_+ and H_-. The fraction of longitudinal polarization is defined as $f_L \equiv |H_0|^2 / (|H_0|^2 + |H_+|^2 + |H_-|^2)$. The observables that distinguish longitudinal from transverse polarization are the helicity angles of the ω mesons, θ_1 and θ_2. The helicity angle for $\omega \to \pi^+\pi^-\pi^0$ is defined as the angle in the ω rest frame between the B^0 momentum and the normal to the decay plane of the three pions.

The time-integrated CP asymmetry is defined as

$$A_{CP} = \frac{\Gamma(\bar{B}^0 \to \omega\omega) - \Gamma(B^0 \to \omega\omega)}{\Gamma(\bar{B}^0 \to \omega\omega) + \Gamma(B^0 \to \omega\omega)}, \qquad (1)$$

where Γ is the partial decay width. This asymmetry can differ for each of the helicity states, $|H_0|^2$, $|H_+|^2$, and $|H_-|^2$.

Theory predictions for the $B^0 \to \omega\omega$ branching fraction ($\mathcal{B}$) are in the range $(0.5$–$3) \times 10^{-6}$; predictions for f_L are in the range $(0.6$–$0.94)$; and A_{CP} could be as large as -70% [18–23]. Experimentally, $B^0 \to \omega\omega$ has been searched for at CLEO-II [24] and at *BABAR* [25]. The latter experiment found evidence for this decay with a significance of 4.4σ. No measurement of f_L or A_{CP} has been reported. In this Letter, we report the first observation of $B^0 \to \omega\omega$ and the first measurements of f_L and A_{CP}.

The data were collected with the Belle detector, which ran at the KEKB [26] e^+e^- asymmetric-energy collider. We analyze the full Belle dataset, which corresponds to an integrated luminosity of 711 fb^{-1} containing $(771.6 \pm 10.6) \times 10^6$ $B\bar{B}$ pairs ($N_{B\bar{B}}$) recorded at an e^+e^- center-of-mass (c.m.) energy corresponding to the $\Upsilon(4S)$ resonance. The Belle detector surrounds the beam pipe and consists of several components: a silicon vertex detector to reconstruct decay vertices; a central drift chamber (CDC) to reconstruct tracks; an array of aerogel threshold Cherenkov counters (ACC) and a barrel-like arrangement of time-of-flight scintillation counters (TOF) to provide particle identification; and an electromagnetic calorimeter (ECL) consisting of CsI(Tl) crystals to identify electrons and photons. All these components are located inside a superconducting solenoid coil providing a 1.5 T magnetic field. An iron flux-return located outside the coil is instrumented to identify muons and detect K_L^0 mesons. More details of the detector can be found in Ref. [27].

We use Monte Carlo (MC) simulated events to optimize selection criteria, calculate signal reconstruction efficiencies, and identify sources of background [28]. MC events are generated using EVTGEN [29] and PYTHIA [30] and

subsequently processed through a detailed detector simulation using GEANT3 [31]. Final-state radiation from charged particles is included using PHOTOS [32]. All analysis is performed using the Belle II software framework [33].

Reconstructed tracks are required to originate from near the e^+e^- interaction point (IP), i.e., have an impact parameter with respect to the IP of less than 4.0 cm along the z direction (that opposite the direction of the positron beam) and of less than 0.5 cm in the transverse (x-y) plane. Tracks are required to have a transverse momentum of greater than 100 MeV/c. To identify pion candidates, a particle identification (PID) likelihood is calculated based upon energy-loss measurements in the CDC, time-of-flight information from the TOF, and light-yield measurements from the ACC [34]. A track is identified as a pion if the ratio $\mathcal{L}(\pi)/[\mathcal{L}(K) + \mathcal{L}(\pi)] > 0.4$, where $\mathcal{L}(K)$ and $\mathcal{L}(\pi)$ are the likelihoods that a track is a kaon or pion, respectively. The efficiency of this requirement is about 97%.

Photons are reconstructed from electromagnetic clusters in the ECL that do not have an associated track. Such candidates are required to have an energy greater than 50 MeV (100 MeV) in the barrel (end-cap) region, to suppress beam-induced background. Candidate π^0's are reconstructed from photon pairs that have an invariant mass satisfying $M_{\gamma\gamma} \in [0.118, 0.150]$ GeV/c^2; this range corresponds to 2.5σ in mass resolution. In subsequent fits, the invariant mass of photon pairs from π^0 candidates are constrained to the nominal π^0 mass [35]. To reduce combinatorial background from low-energy photons, we require that the π^0 momentum be greater than 0.25 GeV/c and that the energies of photon pairs satisfy $|E_{\gamma_1} - E_{\gamma_2}|/(E_{\gamma_1} + E_{\gamma_2}) < 0.9$.

We reconstruct ω candidates from the decay chain $\omega \to \pi^+\pi^-\pi^0$, requiring that the invariant mass satisfy $M(\pi^+\pi^-\pi^0) \in [0.740, 0.820]$ GeV/c^2. This range corresponds to 4.0σ in mass resolution. We reconstruct $B^0 \to \omega\omega$ candidates (B_{sig}^0) from pairs of ω candidates that are consistent with originating from a common vertex, as determined by performing a vertex fit. The ordering of the two ω's is chosen randomly for each event, to avoid an artificial asymmetry in the distribution of helicity angles arising from momentum ordering in the reconstruction. The particles that are not associated with the signal $B^0 \to \omega\omega$ decay are collectively referred as the "rest of the event" (ROE). We reconstruct a decay vertex for the ROE using tracks in the ROE [36].

To suppress background arising from continuum $e^+e^- \to q\bar{q}$ ($q = u, d, s, c$) production, we use a fast boosted decision tree (FBDT) classifier [37] that distinguishes topologically jetlike $q\bar{q}$ events from more spherical $B\bar{B}$ events. The variables used in the classifier consist of modified Fox-Wolfram moments [38]; CLEO "cones" [39]; the magnitude of the ROE thrust [40]; the cosine of the

angle between the thrust axis of B^0_{sig} and the thrust axis of the ROE; the cosine of the angle between the thrust axis of B^0_{sig} and the beam axis; the polar angle of the B^0_{sig} momentum in the e^+e^- c.m. frame; the p value of the B^0_{sig} decay vertex fit; and the separation in z between the B^0_{sig} decay vertex and the vertex of the ROE. The classifier is trained using MC-simulated signal decays and $q\bar{q}$ background events. The classifier has a single output variable C_{FBDT}, which ranges from -1 for unambiguous backgroundlike events to $+1$ for unambiguous signal-like events. We require that $C_{\text{FBDT}} > 0.75$, which rejects approximately 96% of $q\bar{q}$ background while retaining 78% of signal events. The variable C_{FBDT} is transformed to a variable $C' = \log\left[(C_{\text{FBDT}} - 0.75)/(1 - C_{\text{FBDT}})\right]$, which is well modeled by a simple sum of Gaussian functions. The variable C' is subsequently used when fitting for the signal yield, as described below.

To identify B^0_{sig} candidates, we use two kinematic variables: the beam-energy-constrained mass M_{bc} and the energy difference ΔE, defined as

$$M_{\text{bc}} \equiv \frac{1}{c^2}\sqrt{E^2_{\text{beam}} - p^2_B c^2}, \qquad (2)$$

$$\Delta E \equiv E_B - E_{\text{beam}}. \qquad (3)$$

Here, E_{beam} is the beam energy, and E_B and p_B are the energy and momentum, respectively, of the B^0_{sig} candidate. All quantities are evaluated in the e^+e^- c.m. frame. We retain events satisfying $M_{\text{bc}} \in [5.24, 5.29]$ GeV/c^2 and $\Delta E \in [-0.20, 0.20]$ GeV.

Measuring A_{CP} requires identifying the B^0 or $\bar{B}^0$ flavor of B^0_{sig}. The $B^0\bar{B}^0$ pair produced via $e^+e^- \rightarrow \Upsilon(4S) \rightarrow B^0\bar{B}^0$ are in a quantum-correlated state in which the B^0_{sig} flavor must be opposite that of the accompanying B at the time the first B of the pair decays. The flavor of the accompanying B is identified from inclusive properties of the ROE; the algorithm used is described in Ref. [41]. The algorithm outputs two quantities: the flavor q, where $q = +1(-1)$ corresponds to B^0_{sig} being $\bar{B}^0(B^0)$, and a quality factor r ranging from 0 for no flavor discrimination to 1 for unambiguous flavor assignment. For MC-simulated events, $r = 1-2w$, where w is the probability of being mistagged. We do not make a requirement on r but rather divide the data into seven r bins with divisions 0.0, 0.10, 0.25, 0.50, 0.625, 0.75, 0.875, and 1.0.

The fraction of events having multiple candidates is approximately 10%. For these events, the average multiplicity is 2.2. We retain a single candidate by first choosing that with the smallest value of $\chi^2(\pi^0_1) + \chi^2(\pi^0_2)$, where $\chi^2(\pi^0)$ is the goodness of fit resulting from the π^0-mass-constrained fit. If multiple candidates remain after this selection, we choose that with the smallest χ^2 resulting from the $B^0 \rightarrow \omega\omega$ vertex fit. According to MC simulation,

these criteria select the correct B^0_{sig} candidate in 70% of multiple-candidate events.

After these selections, the dominant source of background is continuum production, which does not peak in M_{bc} or ΔE but partially peaks in $M(\pi^+\pi^-\pi^0)$ at m_ω due to $e^+e^- \rightarrow q\bar{q} \rightarrow \omega X$ production. For $e^+e^- \rightarrow B\bar{B}$ background, we find that most of this background does not peak in M_{bc} or ΔE. From MC simulation, we find a small background from $B^0 \rightarrow \omega b_1(1235)^0(\rightarrow \omega\pi^0)$ decays, for which the branching fraction is unmeasured. This background peaks in M_{bc} and at negative values of ΔE; thus, we model this background separately when fitting for the signal yield. Other peaking backgrounds such as $B^0 \rightarrow \omega K^{(*)0}$, $B^0 \rightarrow \omega\eta^{(\prime)}$, $B^0 \rightarrow \omega a_1(1260)^0$, and nonresonant $B^0 \rightarrow \omega\pi^+\pi^-\pi^0$, $B^0 \rightarrow \pi^+\pi^-\pi^0\pi^+\pi^-\pi^0$ decays are negligible [42].

The branching fraction, f_L, and A_{CP} are determined from an extended unbinned maximum likelihood fit to seven observables. The fitted observables are M_{bc}, ΔE, C', the invariant masses of both ω's [denoted $M_1(\pi^+\pi^-\pi^0)$ and $M_2(\pi^+\pi^-\pi^0)$], and the cosine of the helicity angles of both ω's (denoted $\cos\theta_1$ and $\cos\theta_2$). The fit is performed simultaneously for $q = \pm 1$ events and for each of seven r bins. The likelihood function is given by

$$\mathcal{L} = \frac{e^{-\sum_j N_j}}{\prod_k N_k!}\prod_k\left[\prod_{i=1}^{N_k}\left(\sum_j f_{j,k}N_j\mathcal{P}^i_{j,k}\right)\right], \qquad (4)$$

where k indicates the r bin, N_k denotes the total number of events in the kth bin, N_j is the event yield for event category j (j = signal, $q\bar{q}$, nonpeaking $B\bar{B}$ backgrounds, and peaking $B\bar{B}$ backgrounds), $f_{j,k}$ is the fraction of events in the kth bin for category j, and $\mathcal{P}^i_{j,k}$ is the corresponding probability density function (PDF) for event i. The continuum fractions $f_{q\bar{q},k}$ are fixed to values obtained from the data sideband $M_{bc} < 5.265$ GeV/c^2. The $B\bar{B}$ background fractions $f_{B\bar{B},k}$ are fixed to values obtained from MC simulation.

The PDF for the signal component is

$$\mathcal{P}^i_{\text{sig},k} = [1 - q^i\Delta w_k + q^i(1-2w_k)(1-2\chi_d)A_{CP}]$$
$$\times P_{\text{sig},k}(M^i_{\text{bc}}, \Delta E^i, C'^i, M^i_1, M^i_2, \cos\theta^i_1, \cos\theta^i_2), \qquad (5)$$

where $q^i = \pm 1$ is the flavor tag of the ith event, w_k is the mistag fraction for bin k, Δw_k is the difference in mistag fractions between B^0 tags and $\bar{B}^0$ tags, and $\chi_d = 0.1858 \pm 0.0011$ [35] is the time-integrated B^0-$\bar{B}^0$ mixing parameter. The fraction of signal events in the kth bin ($f_{\text{sig},k}$), along with w_k and Δw_k, are determined from data using a control sample of $B^0 \rightarrow D^-(\rightarrow K^+\pi^-\pi^-)\pi^+$ decays, in which the final state is flavor specific (and B^0-$\bar{B}^0$ mixing is accounted

for) [41]. The shape of C' depends slightly on r and thus is parametrized separately for each r bin k.

For longitudinally and transversely polarized signal decays, separate PDFs are used, as their $\cos\theta_{1,2}$ distributions differ. We find that 14.6% (17.6%) of longitudinally (transversely) polarized signal decays have at least one particle misidentified but pass all selection criteria. To account for such misreconstructed signal, each PDF in turn consists of two parts, one for correctly reconstructed signal (denoted "true") and one for misreconstructed signal (denoted "MR"): $P = (1 - f_{\mathrm{MR}})P_{\mathrm{true}} + f_{\mathrm{MR}}P_{\mathrm{MR}}$. The fraction of MR signal (f_{MR}) is fixed from MC simulation.

For correctly reconstructed signal, the M_{bc} distribution is modeled by a Crystal Ball function [43]. The $(\Delta E, M_1, M_2)$ distribution is modeled by a three-dimensional histogram that accounts for correlations among these observables, and C' is modeled by the sum of a Gaussian distribution and a bifurcated Gaussian. The $\cos\theta_{1,2}$ distributions are modeled by a histogram from MC simulation. For misreconstructed signal, $(M_{\mathrm{bc}}, \Delta E)$ is modeled by a two-dimensional histogram that accounts for correlations, and C' is modeled by the sum of two Gaussian functions. The variables $M_{1,2}$ and $\cos\theta_{1,2}$ are modeled by histograms from MC simulation. To account for differences between data and MC simulation, the PDFs for M_{bc}, ΔE, C', and $M_{1,2}$ are adjusted (means slightly shifted, ΔE and $M_{1,2}$ widths scaled by ~15%) according to data-MC differences observed for a control sample of $B^0 \to \bar{D}^0(\to K^+\pi^-\pi^0)\omega$ decays.

For continuum background, correlations among observables are negligible. The M_{bc} distribution is modeled by a threshold ARGUS [44] function, ΔE is modeled by a second-order polynomial, and C' is modeled by the sum of two Gaussian functions. The PDFs for $M_{1,2}$, $\cos\theta_{1,2}$, are divided into two parts to account for true and falsely reconstructed (denoted "non-ω") $\omega \to \pi^+\pi^-\pi^0$ decays,

$$P_{q\bar{q}}(M, \cos\theta) = f_\omega P_\omega(M) P_\omega(\cos\theta)$$
$$+ (1 - f_\omega)P_{\mathrm{non}\text{-}\omega}(M)P_{\mathrm{non}\text{-}\omega}(\cos\theta). \quad (6)$$

The fraction of $q\bar{q}$ background containing true ω decays (f_ω) is floated in the fit. For these decays, M_1 and M_2 are modeled by a histogram from MC simulation, and the $\cos\theta_{1,2}$ distributions are modeled by polynomials. The PDFs for the non-ω component are also taken to be polynomials. All shape parameters except those for C' are floated in the fit; the shape for C' is fixed to that from MC simulation. The PDFs for C' and $M_{1,2}$ for true ω's are adjusted with small calibration factors determined from the $B^0 \to \bar{D}^0(\to K^+\pi^-\pi^0)\omega$ control sample.

For nonpeaking $B\bar{B}$ background, M_{bc} is modeled by a threshold ARGUS function, ΔE is modeled by a second-order polynomial, C' is modeled by the sum of two Gaussian functions, and $M_{1,2}$ and $\cos\theta_{1,2}$ are modeled by histograms from MC simulation. For peaking $B\bar{B}$ background, all PDF shapes are obtained from histograms from MC simulation.

There are a total of 16 floated parameters in the fit: the yields of signal, continuum, peaking $B\bar{B}$, and nonpeaking $B\bar{B}$ backgrounds, the parameters f_L and A_{CP}, and PDF parameters (except that for C') for $q\bar{q}$ background. We fit directly for the branching fraction ($\mathcal{B}$) using the relation between $\mathcal{B}$ and the signal yields,

$$N_L = 2 \times N_{B^0\bar{B}^0} \times \mathcal{B} \times \mathcal{B}_\omega^2 \times f_L \times \varepsilon_L,$$
$$N_T = 2 \times N_{B^0\bar{B}^0} \times \mathcal{B} \times \mathcal{B}_\omega^2 \times (1 - f_L) \times \varepsilon_T, \quad (7)$$

where N_L (N_T) is the yield of longitudinally (transversely) polarized signal and $N_L + N_T = N_{\mathrm{sig}}$, $N_{B^0\bar{B}^0}$ is the number of $B^0\bar{B}^0$ pairs, $\mathcal{B}_\omega = \mathcal{B}(\omega \to \pi^+\pi^-\pi^0) \times \mathcal{B}(\pi^0 \to \gamma\gamma)$, and ε_L and ε_T are the respective signal reconstruction efficiencies for longitudinal and transverse polarization. We take $N_{B^0\bar{B}^0}$ to be $N_{B\bar{B}} \times f^{00}$, where $f^{00} = 0.484 \pm 0.012$ is the fraction of $B^0\bar{B}^0$ production at the $\Upsilon(4S)$ [45]. The efficiencies ε_L and ε_T are obtained from MC simulation and
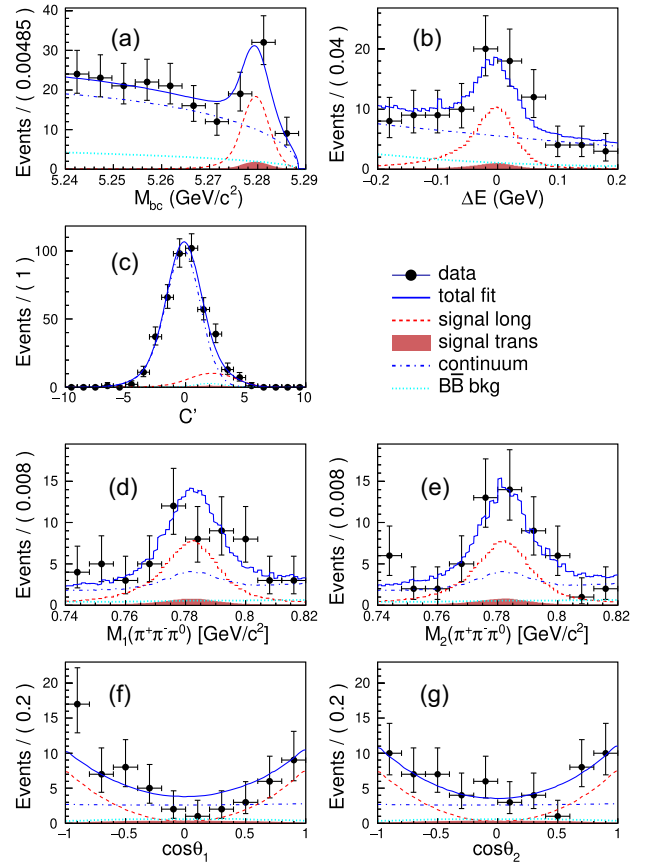

FIG. 1. Projections of the fit for (a) M_{bc}, (b) ΔE, (c) C', (d) $M_1(\pi^+\pi^-\pi^0)$, (e) $M_2(\pi^+\pi^-\pi^0)$, (f) $\cos\theta_1$, and (g) $\cos\theta_2$. Events plotted are in a signal-enhanced region (except for the variable plotted) of $M_{\mathrm{bc}} \in [5.274, 5.290]$ GeV/c^2, $\Delta E \in [-0.080, 0.080]$ GeV, and $C' \in [2, 10]$. The red dashed line shows longitudinally polarized signal; the red-shaded area shows transversely polarized signal; the blue dash-dotted line shows $q\bar{q}$ background; the cyan dotted line shows $B\bar{B}$ background, and the blue solid curve shows the overall fit result.

TABLE I. Systematic uncertainties on $\mathcal{B}$, f_L, and A_{CP}. Those listed in the upper part are additive and included in the significance calculation, as discussed in the text. Those listed in the lower part are multiplicative.

Source	$\mathcal{B}$ (%)	f_L	A_{CP}
Best-candidate selection	3.0	0.07	0.04
Signal PDF	7.7	0.10	0.10
Fit bias	3.0	0.01	0.01
Background PDF	0.7	0.00	0.01
Tracking efficiency	1.4	0.00	0.00
π^0 efficiency	4.0	0.00	0.00
PID efficiency	3.5	0.00	0.00
Continuum suppression	2.4	⋯	⋯
Flavor mistagging	⋯	⋯	0.02
Detection asymmetry	⋯	⋯	0.01
$N_{B^0 \bar{B}^0}$	2.8	⋯	⋯
$\mathcal{B}(\omega \to \pi^+ \pi^- \pi^0) \times \mathcal{B}(\pi^0 \to \gamma\gamma)$	1.6	⋯	⋯
Total	11.4	0.13	0.11

found to be $(8.82 \pm 0.02)\%$ and $(6.54 \pm 0.02)\%$, respectively.

The projections of the fit are shown in Fig. 1. We obtain $N_{\text{sig}} = 60.3 \pm 10.8$, $f_L = 0.87 \pm 0.13$, and $A_{CP} = -0.44 \pm 0.43$. The significance of the signal is evaluated using the difference of the likelihoods for the nominal fit and for a fit with the signal yield set to zero. In the latter case, there are three fewer degrees of freedom: the signal yield, f_L, and A_{CP}. Systematic uncertainties are included in the significance calculation by convolving the likelihood function with a Gaussian function whose width is equal to the total additive systematic uncertainty (see Table I). The signal significance including systematic uncertainties corresponds to 7.9σ.

The systematic uncertainties are summarized in Table I. The uncertainty due to the reconstruction efficiency has several contributions: charged track reconstruction (0.35% per track), π^0 reconstruction (4.0% [46]), PID efficiency (3.5%), and continuum suppression (2.4%). The systematic uncertainty due to continuum suppression is evaluated using the $B^0 \to \bar{D}^0(\to K^+ \pi^- \pi^0)\omega$ control sample: the requirement on C_{FBDT} is varied and the resulting change in the efficiency-corrected yield (2.4%) is assigned as a systematic uncertainty for $\mathcal{B}$. The uncertainty due to the best-candidate selection is evaluated by randomly choosing a candidate; the resulting changes in $\mathcal{B}$, f_L, and A_{CP} are assigned as systematic uncertainties. The systematic uncertainty due to calibration factors for PDF shapes is evaluated by varying these factors by their uncertainties and repeating the fits. The resulting variations in the fit results are assigned as systematic uncertainties. The correlation between ΔE and M_1 and M_2 as found from MC simulation is accounted for in the fit, but there could be differences

between the simulation and data. We thus change this correlation by 10% (absolute) and refit the data; the changes in the fit results are assigned as systematic uncertainties. The fraction of misreconstructed signal is varied by $\pm 30\%$ and the changes from the nominal results are assigned as systematic uncertainties. From a large "toy" MC study, small potential biases are observed in the fit results. We assign these biases as systematic uncertainties. Finally, we include uncertainties on $\mathcal{B}$ arising from $N_{B^0 \bar{B}^0}$ (2.8%) and intermediate branching fractions $\mathcal{B}(\omega \to \pi^+ \pi^- \pi^0) \times \mathcal{B}(\pi^0 \to \gamma\gamma)$ (1.6%) [35].

For A_{CP}, there is systematic uncertainty arising from flavor tagging. We evaluate this by varying the flavor-tagging parameters ε_k, w_k, and Δw_k by their uncertainties; the resulting change in A_{CP} is taken as a systematic uncertainty. To account for a possible asymmetry in backgrounds (arising, e.g., from the detector), we include an $A_{CP}^{q\bar{q}}$ term in the continuum background PDF. We float $A_{CP}^{q\bar{q}}$ in the fit and obtain a value 0.008 ± 0.014, which is consistent with zero. The resulting change in the signal A_{CP} is assigned as a systematic uncertainty. The total systematic uncertainties are obtained by combining all individual uncertainties in quadrature; the results are 11.4% for $\mathcal{B}$, 0.13 for f_L, and 0.11 for A_{CP}.

In summary, we report measurements of the decay $B^0 \to \omega\omega$ using 772×10^6 $B\bar{B}$ pairs produced at the Belle experiment. The branching fraction, fraction of longitudinal polarization, and time-integrated CP asymmetry are measured to be

$$\mathcal{B} = (1.53 \pm 0.29 \pm 0.17) \times 10^{-6}, \tag{8}$$

$$f_L = 0.87 \pm 0.13 \pm 0.13, \tag{9}$$

$$A_{CP} = -0.44 \pm 0.43 \pm 0.11, \tag{10}$$

where the first uncertainties are statistical and the second are systematic. The $B^0 \to \omega\omega$ decay is observed for the first time; the significance including systematic uncertainties is 7.9σ. Our measurements of f_L and A_{CP} are the first such measurements.

Our results for $\mathcal{B}$ and f_L agree well with predictions from next-to-leading-order (NLO) perturbative QCD (PQCD) [23], but not from leading-order (LO) PQCD [19]. This indicates that NLO corrections and power-suppressed terms play an important role in color-suppressed $b \to (u, d)$ decays. Such a role would help clarify the puzzle in $B^0 \to \rho^0 \rho^0$, where the measured f_L is significantly higher than the LO PQCD prediction [19]. Our result for $\mathcal{B}(B^0 \to \omega\omega)$ is significantly higher than the prediction from soft collinear effective theory [22]. Our result for A_{CP} shows no significant CP violation, consistent within uncertainties with CKM unitarity.

---

[1] Charge-conjugate modes are implicitly included throughout this Letter, unless noted otherwise.

[2] N. Cabibbo, Phys. Rev. Lett. **10**, 531 (1963).

[3] M. Kobayashi and T. Maskawa, Prog. Theor. Phys. **49**, 652 (1973).

[4] D. Atwood and A. Soni, Phys. Rev. D **65**, 073018 (2002).

[5] K. F. Chen *et al.* (Belle Collaboration), Phys. Rev. Lett. **91**, 201801 (2003).

[6] B. Aubert *et al.* (*BABAR* Collaboration), Phys. Rev. Lett. **91**, 171802 (2003).

[7] B. Aubert *et al.* (*BABAR* Collaboration), Phys. Rev. Lett. **99**, 201802 (2007).

[8] B. Aubert *et al.* (*BABAR* Collaboration), Phys. Rev. D **78**, 092008 (2008).

[9] M. Prim *et al.* (Belle Collaboration), Phys. Rev. D **88**, 072004 (2013).

[10] H.-N. Li, Phys. Lett. B **622**, 63 (2005).

[11] M. Beneke, J. Rohrer, and D. Yang, Phys. Rev. Lett. **96**, 141801 (2006).

[12] M. Beneke, J. Rohrer, and D. Yang, Nucl. Phys. **B774**, 64 (2007).

[13] S. Baek, A. Datta, P. Hamel, O. F. Hernandez, and D. London, Phys. Rev. D **72**, 094008 (2005).

[14] S.-S. Bao, F. Su, Y.-L. Wu, and C. Zhuang, Phys. Rev. D **77**, 095004 (2008).

[15] I. Adachi *et al.* (Belle Collaboration), Phys. Rev. D **89**, 072008 (2014); **89**, 119903(A) (2014).

[16] R. Aaij *et al.* (LHCb Collaboration), Phys. Lett. B **747**, 468 (2015).

[17] B. Aubert *et al.* (*BABAR* Collaboration), Phys. Rev. D **78**, 071104 (2008).

[18] H.-Y. Cheng and C.-K. Chua, Phys. Rev. D **80**, 114008 (2009).

[19] Z.-T. Zou, A. Ali, C.-D. Lu, X. Liu, and Y. Li, Phys. Rev. D **91**, 054033 (2015).

[20] G. Kramer and W. F. Palmer, Phys. Rev. D **45**, 193 (1992).

[21] Y. Li and C.-D. Lu, Phys. Rev. D **73**, 014024 (2006).

[22] C. Wang, S.-H. Zhou, Y. Li, and C.-D. Lu, Phys. Rev. D **96**, 073004 (2017).

[23] J. Chai, S. Cheng, Y.-h. Ju, D.-C. Yan, C.-D. Lü, and Z.-J. Xiao, Chin. Phys. C **46**, 123103 (2022).

[24] T. Bergfeld *et al.* (CLEO Collaboration), Phys. Rev. Lett. **81**, 272 (1998).

[25] J. P. Lees *et al.* (*BABAR* Collaboration), Phys. Rev. D **89,** 051101 (2014).

[26] S. Kurokawa and E. Kikutani, Nucl. Instrum. Methods Phys. Res., Sect. A **499,** 1 (2003), and other papers included in this volume; T. Abe *et al.*, Prog. Theor. Exp. Phys. **2013,** 03A001 (2013) and references therein.

[27] A. Abashian *et al.* (Belle Collaboration), Nucl. Instrum. Methods Phys. Res., Sect. A **479,** 117 (2002); also see Sec. II in J. Brodzicka *et al.*, Prog. Theor. Exp. Phys. **2012,** 04D001 (2012).

[28] X. Zhou, S. Du, G. Li, and C. Shen, Comput. Phys. Commun. **258,** 107540 (2021).

[29] D. Lange, Nucl. Instrum. Methods Phys. Res., Sect. A **462,** 152 (2001).

[30] T. Sjöstrand, P. Edén, C. Friberg, L. Lönnblad, G. Miu, S. Mrenna, and E. Norrbin, Comput. Phys. Commun. **135,** 238 (2001).

[31] R. Brun *et al.*, CERN Report No. CERN-DD-EE-84-1, 1987.

[32] E. Barberio and Z. Was, Comput. Phys. Commun. **79,** 291 (1994).

[33] M. Gelb *et al.*, Comput. Software Big Sci. **2,** 9 (2018).

[34] E. Nakano, Nucl. Instrum. Methods Phys. Res., Sect. A **494,** 402 (2002).

[35] R. L. Workman *et al.* (Particle Data Group), Prog. Theor. Exp. Phys. **2022,** 083C01 (2022).

[36] W. Waltenberger, W. Mitaroff, F. Moser, B. Pflugfelder, and H. V. Riedel, J. Phys. Conf. Ser. **119,** 032037 (2008).

[37] T. Keck, Comput. Software Big Sci. **1,** 2 (2017).

[38] G. C. Fox and S. Wolfram, Phys. Rev. Lett. **41,** 1581 (1978); the modified moments used in this Letter are described in S. H. Lee *et al.* (Belle Collaboration), Phys. Rev. Lett. **91,** 261801 (2003).

[39] D. M. Asner *et al.* (CLEO Collaboration), Phys. Rev. D **53,** 1039 (1996).

[40] E. Farhi, Phys. Rev. Lett. **39,** 1587 (1977).

[41] F. Abudinén *et al.* (Belle II Collaboration), Eur. Phys. J. C **82,** 283 (2022), we use the category-based algorithm.

[42] The decays $B^0 \to \omega a_1(1260)^0$, $B^0 \to \omega \pi^+ \pi^- \pi^0$, and $B^0 \to \pi^+ \pi^- \pi^0 \pi^+ \pi^- \pi^0$ are currently unmeasured. For this study, we assume branching fractions of 1.0×10^{-5}, which is conservatively large—an order of magnitude larger than $\mathcal{B}(B^0 \to \omega\omega)$.

[43] T. Skwarnicki, Ph.D. thesis, Institute for Nuclear Physics, Krakow, 1986; DESY Internal Report, DESY Report No. F31-86-02, 1986.

[44] H. Albrecht *et al.* (ARGUS Collaboration), Phys. Lett. B **241,** 278 (1990).

[45] S. Choudhury *et al.* (Belle Collaboration), Phys. Rev. D **107,** L031102 (2023).

[46] S. Ryu *et al.* (Belle Collaboration), Phys. Rev. D **89,** 072009 (2014).